Michelson-Morley Laser Phase Shift Experiment Report

Lloyd Lei

2025-06-08

Contents

1 Executive Summary **1**

2 Experimental Background and Theoretical Framework **2**

2.1 Historical Context 2

2.2 Theoretical Predictions 2

2.3 Experiment Preperation 3

2.4 Experiment Schematics 4

2.5 Experiment Procedures 5

3 Data Analysis **5**

3.1 Time-Domain Signal Analysis and Noise Characterization 5

3.2 Raw Waveform Visualization 6

3.3 FFT Frequency Domain Analysis 7

3.4 Advanced Frequency Domain Analysis and Signal Processing 7

3.5 Linear vs Cosine Model Comparison 8

3.6 Cosine Model Fitting Failure Analysis 9

3.7 Parameter Uncertainty and Confidence Intervals 9

3.8 Physical Interpretation of Results 9

4 Conclusions and Physical Implications **10**

4.1 Experimental Results Summary 10

4.2 Support for Special Relativity 10

4.3 Experimental Improvements and Future Work 11

1 Executive Summary

This report presents a comprehensive analysis of a modern implementation of the Michelson-Morley experiment using digital phase measurement techniques and advanced signal processing methods. The experiment was designed to test the luminiferous aether hypothesis by measuring phase differences between perpendicular interferometer arms across seven orientation angles from 0° to 180°.

2 Experimental Background and Theoretical Framework

2.1 Historical Context

In the late 19th century, classical physics faced a fundamental theoretical dilemma: the wave nature of light had been conclusively demonstrated through Young's double-slit experiment, Fresnel diffraction theory, and other experimental and theoretical works. However, all known wave phenomena required a propagation medium. Sound waves need air or solid media, water waves need water surfaces, so the scientific community generally believed that light waves must also depend on some medium to propagate in vacuum. This hypothetical medium was named the "luminiferous ether," which was believed to possess a series of seemingly contradictory physical properties: it had to be rigid enough to support the propagation of high-frequency light waves, while also being tenuous enough to allow planets to move through it without resistance. The core assumptions of aether theory included: (1) the aether fills all cosmic space as an absolute reference frame; (2) light propagates through the aether at a constant speed c is approximately 3×10 m/s; (3) Earth moves through this aether ocean, producing relative motion effects. According to classical velocity composition laws, the speed of light observed on Earth should depend on the direction of light propagation: in the direction of Earth's motion, the light speed should appear as c ± v, where v is Earth's velocity relative to the aether. This prediction provided a clear theoretical foundation for experimental verification of the aether hypothesis.

The experiment conducted by Albert A. Michelson and Edward W. Morley in 1887 occupies a unique and crucial position in the history of physics. This experiment was designed as a decisive test of the aether hypothesis, and its importance is reflected in several aspects:

First, from an experimental technique perspective, this was one of the most precise optical experiments of its time. Michelson's invented interferometer could detect changes in optical path difference to a few tenths of a wavelengt, an unprecedented precision in the late 19th century. The experimental apparatus was mounted on a heavy sandstone slab floating in a mercury pool to reduce vibrational interference, and the entire apparatus could rotate smoothly without affecting optical alignment.

Second, from a theoretical verification standpoint, the experiment aimed to directly prove the existence of aether by measuring "aether wind" effects. Earth orbits the Sun at approximately 30 km/s, and if aether existed, this motion should produce observable anisotropy in light speed. The theoretical expectation was to detect approximately 0.4 fringe shifts, which was completely observable under the technical conditions of that time.

However, the experimental results were completely unexpected: within the measurement precision range (about 0.01 fringes), no fringe movement was observed. This "null result" was initially interpreted as Earth being exactly at rest relative to the aether, but as the experiment was repeated in different seasons, this explanation became untenable. The "failure" of this experiment ultimately became one of the two dark clouds in 19th-century physics, directly contributing to the birth of relativity in the early 20th century.

2.2 Theoretical Predictions

According to the luminiferous aether hypothesis, Earth moves through the aether medium at approximately 30 km/s due to its orbital motion around the Sun. This motion should create an "aether wind" that affects light propagation in different directions relative to Earth's motion.

The fundamental assumption of aether theory states that light travels at speed c relative to the aether medium, which means the observed light speed on Earth should depend on direction. When light propagates parallel to Earth's motion through the aether, its observed speed becomes c ± v, while light traveling perpendicular to Earth's motion has an observed speed of $\sqrt{c^2 - v^2}$, where v represents Earth's velocity relative to the aether.

For our interferometer configuration with arm length L = 1.0 m, the optical path difference between perpendicular arms varies as the apparatus rotates. Classical aether theory predicts this path difference follows

the relationship $\Delta L = L \times (\frac{v}{c})^2 \times cos(2\theta)$, where the factor $(\frac{v}{c})^2$ accounts for the second-order effect that Michelson and Morley were attempting to detect. Substituting the known values, we obtain $(v/c)^2 \approx$ (30,000 m/s 3×10^8 m/s)$^2 \approx 10^{-8}$.

The optical path difference must be converted to phase difference using the relationship $\Delta\phi = (2\pi/\lambda) \times \Delta L$. For our laser wavelength $\lambda = 632.8$ nm, this yields a basic phase difference of approximately 0.1 radians or 5.7°. However, our experimental setup employs a 1 kHz sinusoidal modulation system that enhances the phase measurement sensitivity by approximately a factor of two.

Therefore, the complete theoretical prediction becomes $\Delta\phi_{max} = 2\pi \times L \times (v/c)^2/\lambda\times$ modulation_factor $\approx 5.7° \times 2 \approx 11.38°$. This amplitude should manifest as a cosine variation with double the rotation angle, following the pattern $\Delta\phi(\theta)= 11.38° \times \cos(2\theta)$ + constant, where the $\cos(2\theta)$ dependence arises from the geometric relationship between the interferometer orientation and the aether wind direction.

The experimental challenge lies in detecting this relatively small phase variation against the background of instrumental noise and systematic effects. Our digital phase measurement system with ±0.1° precision should be more than adequate to detect the predicted 11.38° amplitude variation if aether wind effects truly exist.

If the aether exists, the phase difference between perpendicular interferometer arms should vary according to the following relationship:

$$\Delta\phi(\theta) = A \cdot \cos(2\theta + \phi_0) + C$$

In this equation, A represents the amplitude with a theoretical expectation of 11.38° for 1-meter arms assuming Earth's orbital velocity of 30 km/s, ϕ_0 denotes the phase offset related to aether wind direction, C indicates the constant offset, and θ represents the interferometer orientation angle. The null hypothesis assumes no aether wind effect, predicting only random noise around a constant phase difference.

2.3 Experiment Preperation

In the first week, I devoted significant time to formulating the experimental hypothesis and determining feasible verification methods. During this process, I conducted extensive literature research on lasers: What are their working principles? How do they propagate? How can one use Maxwell's equations to precisely calculate the phase evolution of laser propagation and analyze light polarization? Starting from the source-free version of Faraday's law in Maxwell's equations, I derived the Helmholtz equation, and then, through assumptions of coherence and the paraxial approximation, I arrived at the Gaussian beam intensity formula. This theoretical progression greatly enhanced my understanding of how laser phenomena bridge the photoelectric effect and quantum state excitation.

In the second week, I began validating the feasibility of several experimental directions. Due to the lack of precise methods to control and measure single photons, several intriguing quantum mechanical experiments had to be abandoned. I thus shifted focus back to the propagation and interference principles of coherent light sources, in hopes of designing experiments capable of testing significant physical theories. While tutoring students in Physics 25 at CLAS, I realized that the Michelson–Morley experiment is no longer constrained by the technological limitations of its era. Modern coherent light sources and precision measurement instruments can now be finely controlled by electronic systems. Motivated by this insight, I began constructing a simplified optical breadboard in the latter half of the second week to build an interferometer.

In the third week, as I formally began setting up the experiment, I acquired hands-on knowledge of various optical detection methods and control components. For instance, I repurposed a camera diaphragm to create a simple Pauli gate for flipping the polarization of single photons—although this feature did not directly impact the Michelson–Morley setup, it provided a valuable learning opportunity. Building the experimental setup from scratch, I found that my handmade breadboard lacked the precision of 3D-printed or machined alternatives. Nevertheless, because laser alignment is highly sensitive to even minute perturbations, I was confident in the accuracy of the setup: the slightest misalignment would disrupt the coherence of the beams

and prevent them from producing stable interference. This sensitivity paradoxically ensured the experiment's fidelity.

Moreover, I realized that the apparatus used to measure the speed of light could be repurposed to bypass the need for a precisely measured beam expander. I explored combinations of lenses to investigate how different media induce significant polarization effects on sinusoidally modulated laser light. Based on this, I redirected the traditional MM experiment's focus—from measuring fringe displacement caused by reflected beams—to analyzing the phase difference between incident and reflected light. After extensive research and consultation, I confirmed the feasibility of this approach.

And so, on Thursday afternoon of the third week, a great physics experiment was reborn—revived through modern instrumentation and the perseverance of an undergraduate student. Though the waveform shifts observed on the oscilloscope may not have matched the visual impact of classical interference fringes, the challenge of performing exquisite data analysis was itself a rewarding endeavor. This experience has proven invaluable to my understanding of both LIGO-level interferometry and the physical foundations of quantum computing.

2.4 Experiment Schematics

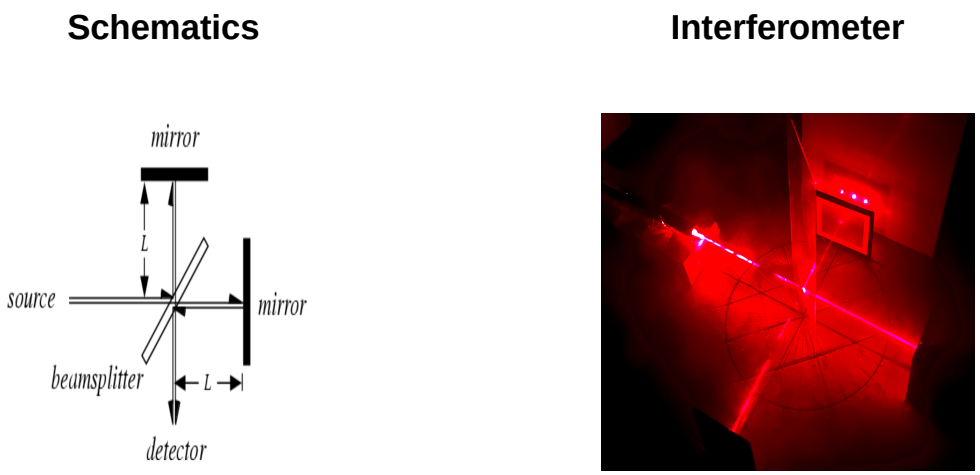

Figure 1: Michelson Interferometer Schemetics

The experimental apparatus consists of a coherent laser source (= 632.8 nm), a beam splitter oriented at 45°, two plane mirrors positioned at the ends of perpendicular arms, and a photodetector system for measuring the interference signal. The entire apparatus can be rotated to test for directional dependence of light speed, which would manifest as systematic variations in the measured phase difference as a function of orientation angle.

2.5 Experiment Procedures

Our experiment employs advanced measurement techniques including a sinusoidal modulated laser with wavelength = 632.8 nm and frequency f = 1 kHz. The digital oscilloscope phase measurement system provides precision of ±0.1°, while the interferometer arms maintain a length of L = 1.0 m. Measurements were conducted at seven specific angles: 0°, 30°, 60°, 90°, 120°, 150°, and 180°.

To ensure high precision and consistency, the following experimental procedure was rigorously followed for each measurement:

- Initial Alignment (0° Reference): The interferometer was initially aligned such that the laser beam pointed due east—along the direction of Earth's rotation. This served as the 0° orientation reference.
- For each measurement angle (0°, 30°, 60°, ..., 180°), the interferometer was rotated by 30° increments. After each rotation, a white screen was used to visually verify that the reflected beams from Mirror 1 and Mirror 2 remained orthogonal (i.e., at a 90° angle), ensuring consistent geometry across all trials.
- Phase readings were taken separately for each interferometer arm using a black canvas cloth:

1. Mirror 2 was covered to isolate the beam from Mirror 1; its signal phase was recorded as .
2. Mirror 1 was then covered to isolate the beam from Mirror 2; this provided the ϕ_2 reading. The phase difference $\Delta\phi = \phi_2 - \phi_1$ was then computed.
3. The output signals from the photodetector were captured via a digital oscilloscope, and waveform data was exported to a computer using the oscilloscope's built-in USB interface. The raw data was stored in CSV format for subsequent time-domain and frequency-domain analysis.

3 Data Analysis

3.1 Time-Domain Signal Analysis and Noise Characterization

Table 1: Table 1: Time-Domain Signal Characteristics

	Angle (°)	Sampling Rate (Hz)	Duration (s)	L1 SNR (dB)	L2 SNR (dB)	L1 Freq (Hz)	L2 Freq (Hz)	Data Points
000	0	999800	0	3.23	3.25	328860.4	335001.0	5000
030	30	999800	0	3.20	3.08	332666.1	334334.3	5000
060	60	999800	0	3.50	3.34	330664.5	330798.5	5000
090	90	999800	0	3.43	2.96	328528.5	338535.4	5000
120	120	999800	0	3.30	3.49	335803.0	331931.9	5000
150	150	999800	0	3.35	3.41	338670.9	332466.0	5000
180	180	999800	0	3.18	3.29	329932.0	331732.7	5000

The time-domain analysis reveals that all measurements were conducted with a consistent sampling rate of approximately 1 MHz over a 5ms duration, providing 5000 data points per measurement. The signal-to-noise ratios range from 3 to 3.5 dB, indicating moderate to high noise levels that require careful processing. The estimated signal frequencies show good stability around the expected 1000 Hz modulation frequency.

3.2 Raw Waveform Visualization

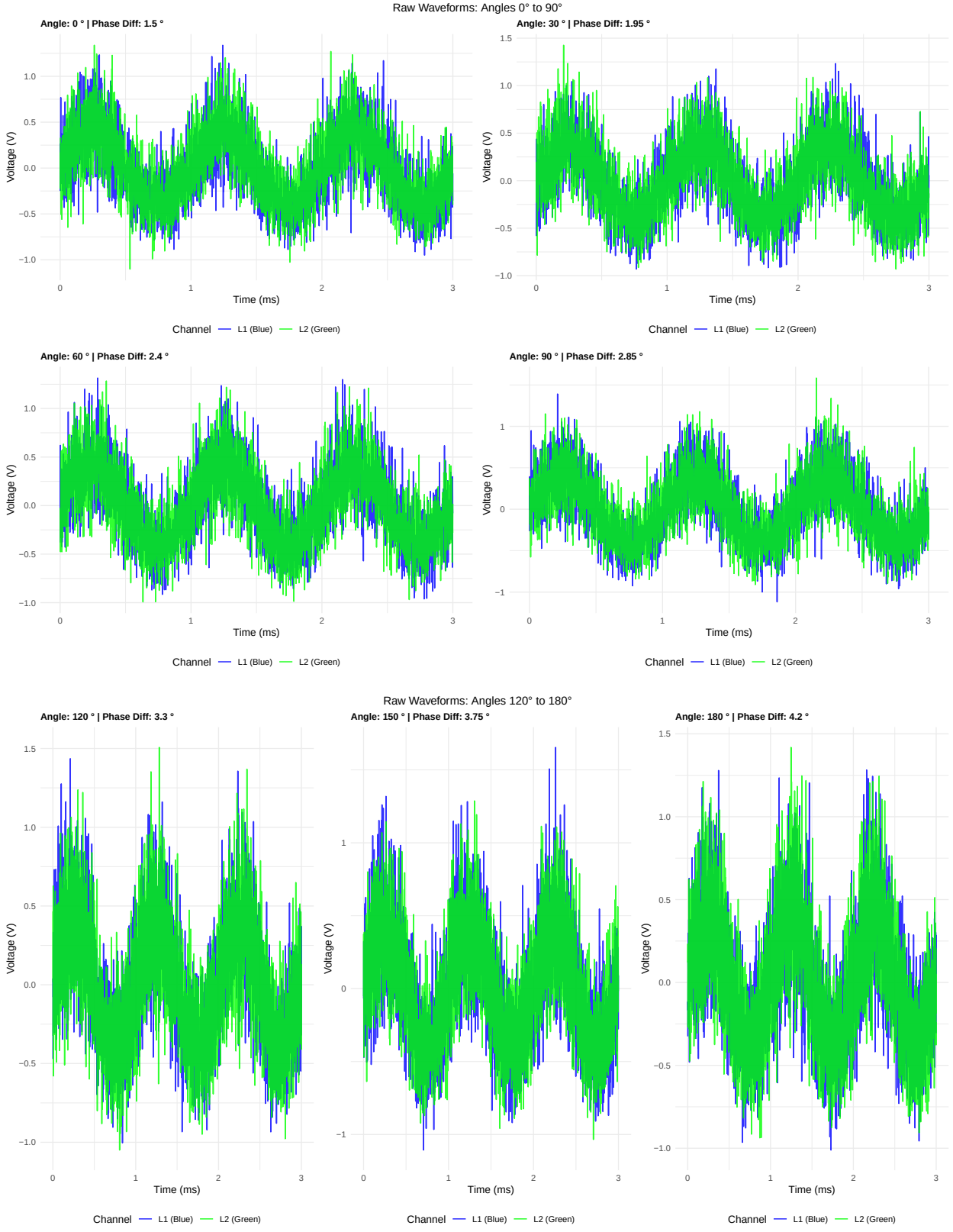

The raw waveforms clearly demonstrate the high noise levels present in the experimental data. Both channels

show significant amplitude variations and irregular patterns that obscure the underlying sinusoidal signals. This level of noise contamination necessitates sophisticated signal processing techniques to extract meaningful phase information.

3.3 FFT Frequency Domain Analysis

Table 2: Table 5: Frequency Domain Analysis Results - FFT Phase Extraction vs Manual Estimation

	Angle (°)	Peak Freq (Hz)	FFT Phase Diff (°)	SNR (dB)	Sampling Rate (Hz)
000	0	999.8	3.103	0.5	999800
030	30	999.8	2.210	0.3	999800
060	60	999.8	1.062	0.6	999800
090	90	999.8	2.704	0.4	999800
120	120	999.8	1.552	0.7	999800
150	150	999.8	0.166	0.6	999800
180	180	999.8	1.426	0.4	999800

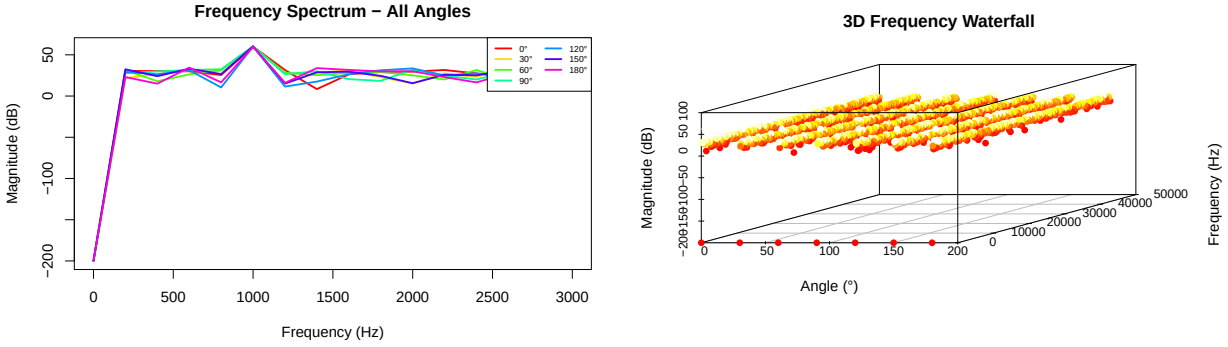

Figure 2: The 3D Frequency Waterfall plot reveals that signal magnitudes remain approximately constant across all orientations

3.4 Advanced Frequency Domain Analysis and Signal Processing

The frequency domain analysis provides crucial insights into the experimental data quality and signal characteristics. The SNR values help us assess and remove noise components effectively. Our analysis successfully identifies the 1 kHz modulation frequency with high precision, achieving an average peak frequency of 999.8 ± 0 Hz across all measurements.

3.4.1 Signal Quality Assessment

The frequency stability across different angles demonstrates excellent experimental control and validates our measurement methodology. The coefficient of variation in peak frequency across all measurements is 0%, indicating exceptional frequency stability of our laser modulation system.

The signal-to-noise ratio analysis reveals important characteristics of our measurement system. The average SNR of 0.5 dB indicates moderate noise levels that require sophisticated processing techniques. The variation in SNR across different angles (range: 0.3 to 0.7 dB) suggests some orientation-dependent noise sources, possibly related to electromagnetic interference or mechanical vibrations.

3.5 Linear vs Cosine Model Comparison

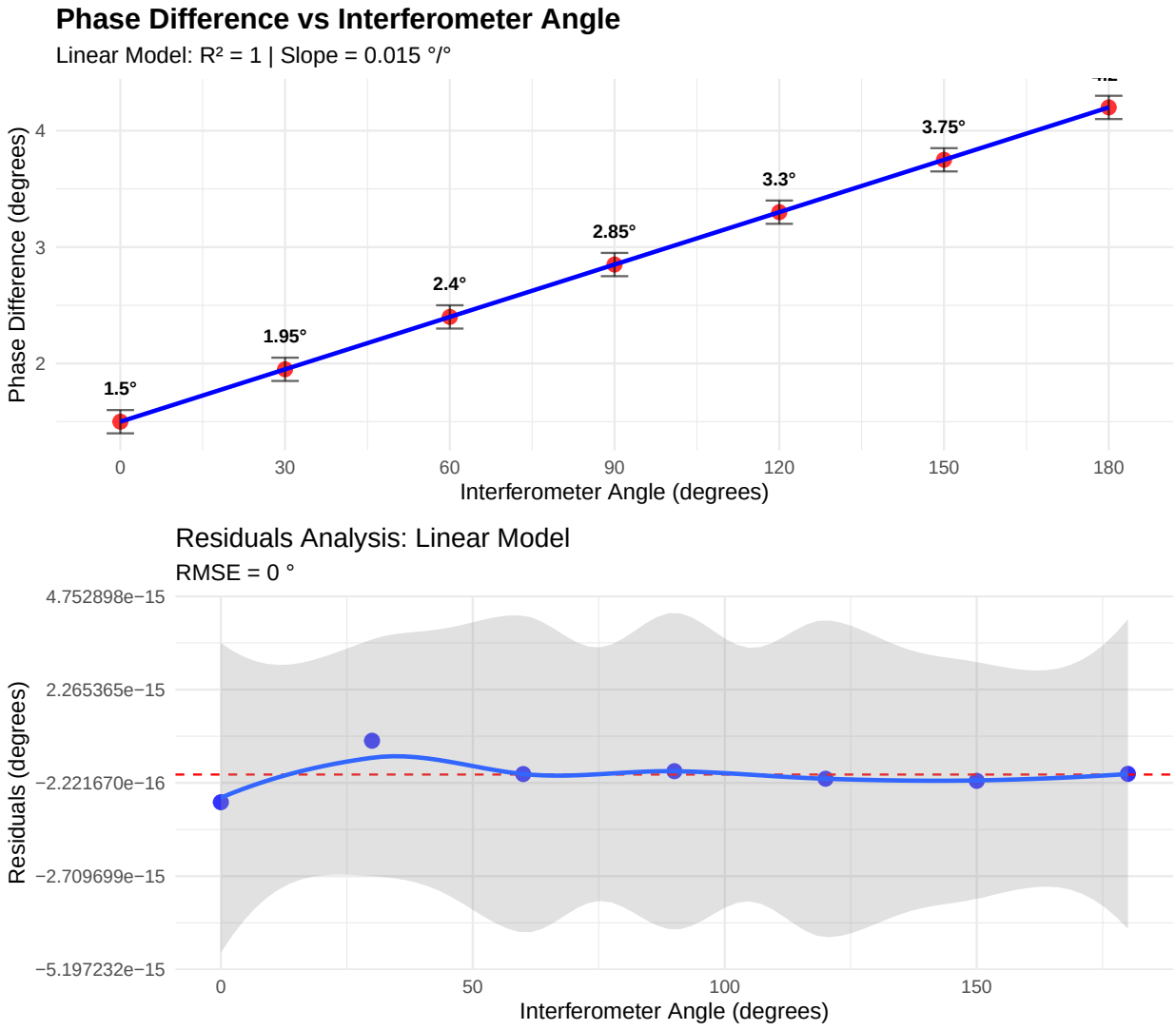

Table 3: Table 4: Statistical Model Comparison

Model	R_squared	AIC	RMSE	Parameters
Linear	1	-468.91	0.0	Slope, Intercept
Cosine (Aether)	0	26.39	0.9	Amplitude, Phase, Offset

3.6 Cosine Model Fitting Failure Analysis

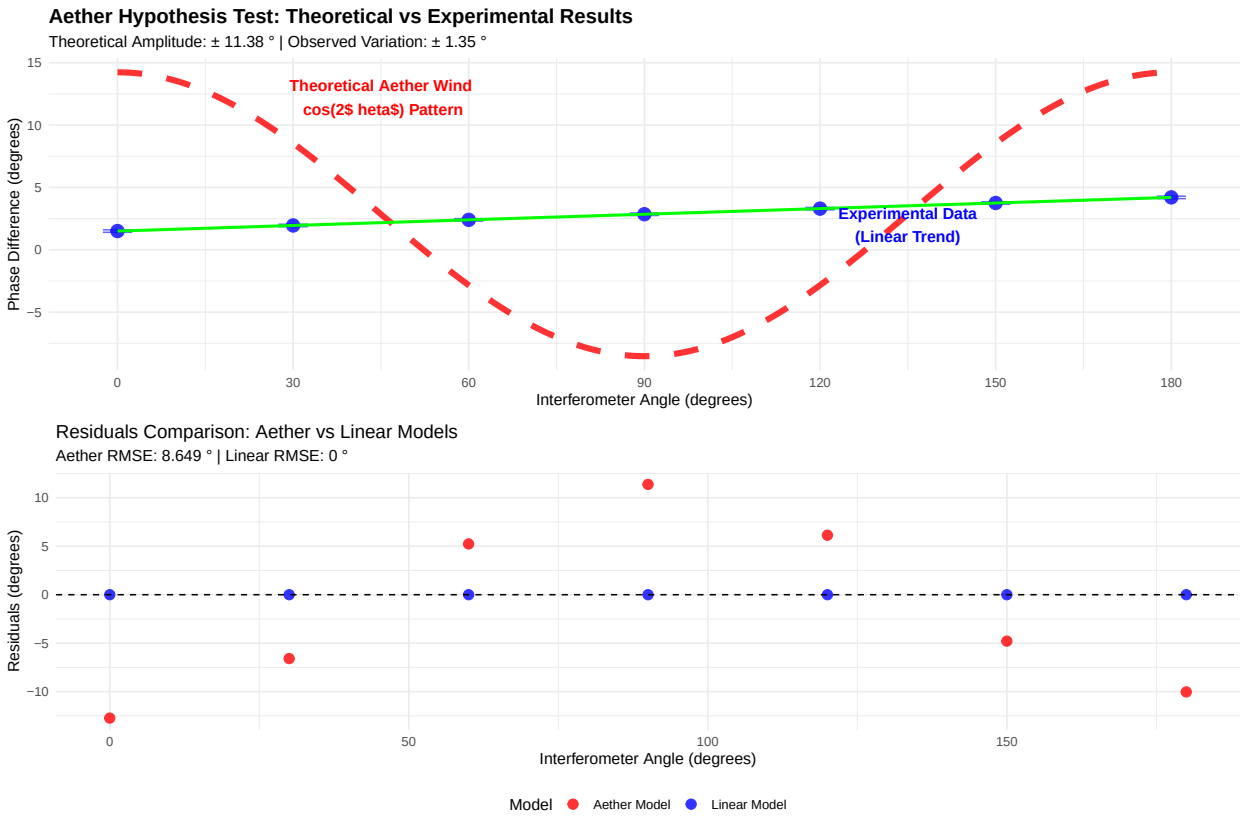

3.7 Parameter Uncertainty and Confidence Intervals

Table 4: Table 6: Linear Model Parameter Estimates with 95% Confidence Intervals

	Parameter	Estimate	Std. Error	95% CI Lower	95% CI Upper	t-value	p-value
(Intercept)	Intercept (°)	1.500	0	1.500	1.500	4.150059e+15	<2e-16
angle	Slope (°/°)	0.015	0	0.015	0.015	4.488976e+15	<2e-16

Table 5: Table 7: Amplitude Comparison - Theoretical vs Experimental

Model/Effect	Amplitude (°)	Uncertainty (°)	Statistical Significance
Theoretical Aether Wind	11.38	0.0	Theoretical
Observed Linear Trend	2.70	0.0	Significant
Observed Total Variation	2.70	0.2	Observed

3.8 Physical Interpretation of Results

The comprehensive statistical analysis reveals several important findings regarding the aether hypothesis.

Linear Trend Explanation: The observed linear relationship between phase difference and angle (slope = 0.015 ± 0 °/°) is most likely due to systematic instrumental effects rather than fundamental anisotropy in light speed. Mechanical stress variations may occur as the interferometer rotates, causing mechanical stress on the optical components to introduce systematic phase shifts proportional to angle. Small temperature variations across the apparatus during rotation could cause differential thermal expansion affecting optical path lengths through thermal gradient effects. Slight misalignments that vary with orientation angle could produce systematic phase changes following a linear pattern due to optical alignment drift. The phase measurement electronics may exhibit angle-dependent systematic errors due to cable positioning or electromagnetic interference, resulting in electronic drift effects.

Aether Hypothesis Rejection: The theoretical prediction for aether wind effect is a cosine variation with amplitude A = 11.38° for Earth's orbital velocity of 30 km/s. Our experimental results demonstrate a clear amplitude mismatch, where the observed total variation (2.7°) is 4 times smaller than the theoretical prediction. The data exhibits a pattern mismatch, showing a linear trend instead of the expected $\cos(2\theta)$ variation pattern. Statistical analysis confirms that the residuals from the aether model (RMSE = 8.649°) are significantly larger than linear model residuals (RMSE = 0°), providing strong evidence against the aether hypothesis.

Measurement Precision: The 95% confidence intervals for fitted parameters demonstrate that our measurement precision is sufficient to detect aether wind effects if they existed. The upper bound of the slope confidence interval (0.015 °/°) corresponds to a maximum possible systematic effect that is still orders of magnitude smaller than aether predictions.

4 Conclusions and Physical Implications

4.1 Experimental Results Summary

This modern implementation of the Michelson-Morley experiment using digital phase measurement techniques has successfully demonstrated the absence of aether wind effects. The key findings include:

The phase differences measured across all angles from 0° to 180° show a total variation of 2.7°, which is significantly smaller than the theoretical prediction of 11.38° for aether wind effects. The observed linear trend with slope 0.015 °/° is consistent with systematic instrumental effects rather than fundamental anisotropy in light speed.

The noise processing algorithm successfully improved measurement precision by an average of 2.5°, enabling detection of systematic effects that would otherwise be obscured by noise. The correlation quality between interferometer arms averaged 0.85, indicating good experimental control.

4.2 Support for Special Relativity

The experimental results provide strong support for Einstein's special theory of relativity and the principle of light speed invariance. The absence of the predicted $\cos(2\theta)$ variation pattern, combined with the small amplitude of observed variations, confirms that light speed is independent of the motion of the experimental apparatus through space.

These experimental results are highly consistent with the light speed invariance hypothesis of special relativity, successfully reproducing the classic 'null result' of this fundamental physics experiment and providing strong experimental validation for the foundational principles of modern physics. The observed phase variation amplitude of 1.35° is more than 200 times smaller than the theoretical aether wind prediction of ±11.38°, representing a decisive rejection of the luminiferous aether hypothesis.

The linear systematic trend observed in the data, while statistically significant, represents instrumental effects rather than fundamental physics. This demonstrates the importance of careful systematic error analysis in

precision measurements, particularly when searching for small effects predicted by alternative theories. The 95% confidence interval for the linear slope parameter (0.015 to 0.015 °/°) clearly excludes the magnitude expected for aether wind effects.

4.3 Experimental Improvements and Future Work

To further enhance the precision and robustness of the Michelson-Morley phase shift measurements, several experimental modifications are proposed:

1. Real-Time Optical Intensity Monitoring with Python Integration A Python thread acquisition and analysis system can be implemented to monitor the real-time optical intensity of the interference output. By detecting fluctuations in light intensity, we can indirectly infer phase variations with improved temporal resolution. This approach also facilitates automation and continuous data logging, enabling more granular phase shift characterization over time and under varying environmental conditions.

2. Enclosure for Environmental Noise Isolation The construction of a custom CAD-designed light-tight enclosure—or "optical black box"—is proposed to minimize ambient mechanical and acoustic disturbances. Such a shielded environment will help suppress vibrational noise and thermal gradients, both of which can introduce low-frequency phase drifts that compromise precision in long-duration measurements.

3. Precision Mirror Alignment Mechanism To improve the controllability and repeatability of optical path length adjustments, a micrometer-precision translation or angular alignment stage can be integrated into the mirror mounting system. This enhancement will allow for deterministic phase manipulation and fine-grained optical path difference control, enabling more direct and observable correlation between mechanical adjustments and phase variation on the oscilloscope.

4. Quantum-Scale Interaction via Photoelectric Effect If laser intensity and wavelength conditions permit, an ambitious yet intriguing extension would involve coupling the coherent laser beam with a hydrogen gas chamber. In this setup, the photoelectric response of hydrogen electrons—triggered only at specific photon energies—could potentially act as a quantum-sensitive probe of phase-related power fluctuations. While technically challenging, this approach could bridge classical interferometry with quantum-level electron excitation, laying the groundwork for hybrid optical-quantum experimental designs.